Arabian Journal of Chemistry (2022) **15**, 104178

King Saud University

Arabian Journal of Chemistry

www.ksu.edu.sa
www.sciencedirect.com

ORIGINAL ARTICLE

Modification of sodium aluminum silicate hydrate by thioglycolic acid as a new composite capable of removing and preconcentrating Pb(II), Cu(II), and Zn(II) ions from food and water samples

Asma S. Al-Wasidi [a], Ahmed M. Naglah [b,c], Fawaz A. Saad [d], Ehab A. Abdelrahman [e,*]

[a] *Department of Chemistry, College of Science, Princess Nourah Bint Abdulrahman University, P.O. Box 84428, Riyadh 11671, Saudi Arabia*
[b] *Department of Pharmaceutical Chemistry, Drug Exploration & Development Chair (DEDC), College of Pharmacy, King Saud University, P.O. Box 2457, Riyadh 11451, Saudi Arabia*
[c] *Peptide Chemistry Department, National Research Centre,12622-Dokki, Cairo, Egypt*
[d] *Department of Chemistry, Faculty of Applied Sciences, Umm Al-Qura University, Makkah 21955, Saudi Arabia*
[e] *Chemistry Department, Faculty of Science, Benha University, Benha 13518, Egypt*

Received 23 May 2022; accepted 7 August 2022
Available online 10 August 2022

KEYWORDS

Sodium aluminum silicate hydrate;
Thioglycolic acid;
Novel composite;
Adsorption;
Heavy metals;
Preconcentration

Abstract In this paper, sodium aluminum silicate hydrate was synthesized using rice husk as a silicon source and scrap aluminum cans as an aluminum source. Afterward, with the aid of microwave heating, a composite of sodium aluminum silicate hydrate and (3-aminopropyl)trimethoxysilane was facilely synthesized then modified by thioglycolic acid to produce a new composite. Besides, characterization of the synthesized composite was carried out using XRD, FT-IR, TEM, CHN elemental analyzer, nitrogen gas sorption analyzer, and SEM. The XRD pattern of the produced composite shows that there is a halo at $2\theta = 25.0°$, which means that there is a crystalline structure that is combined with an amorphous background. The SEM and TEM studies indicate that the synthesized composite has a structure similar to cotton. The synthesized composite was utilized for the efficient removal and preconcentration of Pb(II), Cu(II), and Zn(II) ions from food and water samples prior to determination by flame atomic absorption spectrometry. The produced composite has

* Corresponding author.
E-mail addresses: dr.ehabsaleh@yahoo.com, ehab.abdelrahman@fsc.bu.edu.eg (E.A. Abdelrahman).

Peer review under responsibility of King Saud University.

Production and hosting by Elsevier

https://doi.org/10.1016/j.arabjc.2022.104178

a maximum adsorption capacity of 185.53, 168.92, and 125.94 mg/g for Pb(II), Cu(II), and Zn(II) ions, respectively. The recovery findings demonstrate that the process is accurate, adaptable, and resulted in quantitative separation (greater than95 percent). Furthermore, the % RSD was less than 3.5 percent, indicating good reproducibility. The Langmuir isotherm and pseudo-second-order model fit the experimental results well. The thermodynamic studies established that the adsorption process is spontaneous, chemical, and exothermic. The produced composite was successfully regenerated and used multiple times to remove the metal ions under investigation from aqueous solutions.

1. Introduction

Zinc and copper are important elements for humans because they play a role in a number of biological processes (Rani et al., 2021; Takahashi, 2022). Numerous disorders are associated with an imbalance of zinc and copper in the human body (Covre et al., 2022; Disilvestro et al., 2012; Li et al., 2021). In comparison, Lead is not recognized to have any known biological roles. Lead poisoning has the greatest effect on the renal, reproductive, and neurological systems (Słota et al., 2022). Numerous techniques were used for the identification of metal ions including electrothermal atomic absorption spectrometry (ETAAS), flame atomic absorption spectrometry (FAAS), inductively coupled plasma mass spectrometry (ICP-MS), and inductively coupled plasma optical emission spectrometry (ICP-OES) (Chen et al., 2018). In the majority of cases, a preconcentration method is necessary to increase the instrument's sensitivity and remove any matrix interference (Ahmad et al., 2020). Cloud point extraction, dispersive solid phase extraction, and liquid–liquid microextraction are the most frequently used separation procedures (Iqbal et al., 2020; Mandal and Lahiri, 2022; Ramezani et al., 2022). The dispersive solid phase extraction is distinguished by its ease of use, reproducibility, and selectivity (Abdelrahman and Hegazey, 2019a, 2019b). Recently, there has been a surge of interest in the development of effective adsorbents for a variety of contaminants derived from agricultural wastes (Abdelrahman et al., 2021). The biosorbents feature a porous structure that include functional groups, for example, COOH and OH that can be modified to enhance their capacity for adsorption (Dai et al., 2018). Rice husk is a byproduct of rice milling with an annual output capacity of around 500 tons (Seliem et al., 2016). The majority of this quantity gets disposed of improperly, particularly in developing nations, endangering the environment's safety (Zhang et al., 2021). Rice husk, which is composed primarily of silica (approximately 20 %), cellulose (about 55 %), and lignin (approximately 22 %), has been employed as a source of silica in the creation of mesoporous silica and zeolite compounds (Abdelrahman et al., 2021; Kamari and Ghorbani, 2021). Rice husk-based materials were enhanced with polypyrrole, diethanolamine, and sulfuric acid or nitric acid/potassium carbonate treatment to serve as effective substances for the removal of metal ions (Akhtar et al., 2010; El-Shafey, 2010; Xiong et al., 2019). Additionally, untreated Rice husk ash was employed to adsorb metal ions from aqueous solutions (Saeed et al., 2022). Also, various zeolite nanoparticles were synthesized from aluminum wastes (Abdelrahman, 2018; Abdelrahman and Hegazey, 2019a, 2019b). Adsorption with environmentally acceptable materials is an extremely forward-thinking technology for the removal of organic and inorganic contaminants from aqueous solutions, particularly when zeolites or geopolymers derived from solid wastes are used. Recent studies have concentrated on the use of zeolites or geopolymers as environmentally beneficial nanoadsorbents owing to their high efficiency, stability, ease of manufacture, great binding property, and low cost (Abdelrahman, 2018; Abdelrahman and Hegazey, 2019a, 2019b). Microwave irradiation is currently widely utilized in chemical synthesis because it has several advantages over conventional heating (Wang et al., 2021). The advantages usually involve accelerated reaction times, pure samples, high yields, and security. Microwave heating works by directing energy via the container's walls and heating only the components of the vessel. Because the heating is homogeneous, there are undesirable by-products and the potential of particle agglomeration is minimized (Liu et al., 2021). Despite these benefits, microwave heating is only used in a restricted number of cases to modify adsorbents for dispersive solid phase extraction. The use of microwave to modify the compounds resulted in more effective compounds than those generated using reflux method (Hussain et al., 2022; Naeimi et al., 2022). In this work, sodium aluminum silicate hydrate was facilely synthesized according to our previous work by Ehab et al. exploiting rice husk as a silicon source and waste aluminum cans as an aluminum source (Abdelrahman et al., 2021). After that, a composite of sodium aluminum silicate hydrate with (3-aminopropyl)trimethoxysilane was facilely synthesized then modified by thioglycolic acid as a novel composite by the aid of microwave heating. The paper's novel aspect stems from the loading of thioglycolic acid on sodium aluminum silicate hydrate, where this acid has hydroxyl and thiol functional groups, which can react with metal ions to produce chelates. Thus, it is expected that this new composite will be promising in extracting metal ions from aqueous solutions. The sodium aluminum silicate hydrate/thioglycolic composite was identified utilizing XRD, FT-IR, TEM, CHN elemental analyzer, nitrogen gas sorption analyzer, and SEM. The synthesized solid phase was operated for the removal and preconcentration of Pb(II), Zn(II), and Cu(II) ions from aqueous solutions using the batch protocol. The proposed dispersive solid phase extraction method was employed for preconcentration of studied metal ions from real samples before analysis by flame atomic absorption spectrometry.

2. Experimental

2.1. Chemicals

Sodium hydroxide (NaOH), (3-aminopropyl)trimethoxysilane ($C_6H_{17}NO_3Si$), thioglycolic acid ($C_2H_4O_2S$), hydrochloric acid (HCl), toluene (C_7H_8), ethanol (C_2H_6O), lead(II) nitrate ($Pb(NO_3)_2$), zinc(II) chloride heptahydrate ($ZnCl_2{\cdot}6H_2O$), copper(II) chloride dihydrate ($CuCl_2{\cdot}6H_2O$), potassium chloride (KCl), ethylenediaminetetraacetic acid disodium salt dihydrate ($C_{10}H_{16}N_2Na_4O_{10}$), nitric acid ($HNO_3$), and thiourea ($CH_4N_2S$) were obtained from Sigma Aldrich Company (Purity = 99.99 %) and consumed as received without any additional purification. The rice husk was collected from a rice mill located near the Egyptian city of Menia Alqamh. Besides, aluminum cans were collected from a local market in Benha city, Egypt.

2.2. Synthesis of composite

Firstly, the sodium aluminum silicate hydrate sample was prepared according to our previous work by Ehab et al. exploiting rice husk as a silicon source and waste aluminum cans as an aluminum source (Abdelrahman et al., 2021; Al-wasidi et al., 2022; Al-Wasidi et al., 2022a). For obtaining rice husk ash, the rice husk was burnt at 700 °C for 7.00 hrs. Also, 2.50 g of rice husk ash was refluxed for 2.00 hrs using a 100.00 mL of 1.50 M sodium hydroxide solution for obtaining the silicon solution. Besides, 1.00 g of the outer part of aluminum cans was refluxed for 30 min using a 55.00 mL of 2.10 M sodium hydroxide solution for obtaining the aluminum solution. Moreover, the aluminum solution was added drop by drop to the silicon solution with continual stirring for 1.50 hrs. Furthermore, the mixture was heated until 75 mL remained then the remaining volume was hydrothermally treated for 12.00 hrs at 150.00 °C using a 100.00 mL Teflon-lined autoclave. The white precipitate formed was filtered using a centrifuge, washed carefully with hot distilled water and ethanol, and dried for 24 hrs at 60 °C. The novel composite of sodium aluminum silicate hydrate with (3-aminopropyl)trimethoxysilane was prepared according to our previous work by Khalifa et al. with some changes (Khalifa et al., 2020). 2.00 g of the sodium aluminum silicate hydrate and 2.20 mL of (3-aminopropyl)trimethoxysilane were mixed then refluxed for 24 hrs at 120 °C using a 50.00 mL toluene. The obtained composite was filtered using a centrifuge, washed carefully with hot distilled water and ethanol, and dried for 24 hrs at 60 °C. Additionally, 1.00 g of sodium aluminum silicate hydrate/(3-aminopropyl)trimethoxysilane composite, 1.00 mL of thioglycolic acid, and 60.00 mL of toluene were mixed then transferred into a 100.00 mL Teflon-lined autoclave to hydrothermally treated for 3.00 hrs at 120.00 °C using a domestic microwave oven (Abdelrahman et al., 2021; Al-wasidi et al., 2022; Al-Wasidi et al., 2022a). The formed product was filtered using a centrifuge, washed carefully with hot distilled water and ethanol, and dried for 24 hrs at 60 °C. The processes involved in the synthesis of sodium aluminum silicate hydrate/(3-aminopropyl)trimethoxysilane/thioglycolic acid composite are summarized in Scheme 1 (Abdelrahman et al., 2021; Al-wasidi et al., 2022; Al-Wasidi et al., 2022a).

2.3. Instruments

X-ray diffraction patterns of the synthesized samples were obtained utilizing D_8 Advance X-ray diffractometer adopting copper target with K_α line have a wavelength equal to 0.15 nm. Infrared spectra of the synthesized samples were obtained using KBr disc in the range from 4000 to 400 cm^{-1} utilizing a Nicolet FT-IR spectrometer. A Quantachrome NOVA touch LX_2 nitrogen gas sorption analyzer was employed for the measurement of the average pore radius, BET surface area, and total pore volume of the synthesized samples. The surface morphology and EDX spectra of the synthesized samples were obtained utilizing a JEOL 2000 Scanning electron microscope. The morphologies of the synthesized samples were obtained utilizing an EM-2100 high-resolution transmission electron microscope. A PerkinElmer CHN Elemental Analyzer was utilized for the measurement of the CHN percent of the synthesized composite. The concentration of studied metal ions was determined utilizing a 210 Buck Scientific atomic absorption spectrometer equipped with an acetylene–air flame. The wavelengths for lead, zinc, and copper were 283.30, 213.90, and 324.80 nm, respectively whereas a spectral bandwidth equals 7 Å.

2.4. Extraction of Cu(II), Pb(II), and Zn(II) ions from aqueous solutions

The effect of pH was studied as the following; 50 mg of the synthesized composite were mixed with 80 mL of 120 mg/L of the studied metal ion at adapted pH (2.00–8.00). After 180 min of stirring, the mixture was filtered. An atomic absorption spectrometer was used to determine the remaining concentration of the examined metal ion in the filtrate. The pH of the metal ion solution was adjusted using 0.1 M NaOH or HCl. A value higher than pH = 8 has not been studied for the occurrence of precipitation, which makes the % removal as a result of adsorption unreal. The effect of time was studied as the following; 50 mg of the synthesized composite were mixed with 80 mL of 120 mg/L of the studied metal ion at pH = 6 for varied times (5–120 min). After stirring at specified times, the mixture was filtered. An atomic absorption spectrometer was used to determine the remaining concentration of the examined metal ion in the filtrate. The effect of temperature was studied as the following; 50 mg of the synthesized composite were mixed with 80 mL of 120 mg/L of the studied metal ion at pH = 6 for varied temperatures (298–323 K). After stirring for 80 min, the mixture was filtered. An atomic absorption spectrometer was used to determine the remaining concentration of the examined metal ion in the filtrate. The effect of concentration was studied as the following; 50 mg of the synthesized composite were mixed with 80 mL of varied concentrations (5–180 mg/L) of the studied metal ion at pH equals 6. After stirring for 80 min, the mixture was filtered. An atomic absorption spectrometer was used to determine the remaining concentration of the examined metal ion in the filtrate. Eq. (1) was utilized to determine the quantity of extracted Pb(II), Zn(II), or Cu(II) ions per gram of the synthesized composite (Q, mg/g).

$$Q = [C_i - C_e] \times \frac{V}{M} \tag{1}$$

Eq. (2) was utilized to determine the % removal (% R) of Zn(II), Pb(II), or Cu(II) ions.

$$\%R = \frac{C_i - C_e}{C_i} \times 100 \tag{2}$$

C_i (mg/L) denotes the starting concentration of Zn(II), Pb (II), or Cu(II) ions. Besides, C_e (mg/L) denotes the equilibrium concentration of Zn(II), Pb(II), or Cu(II) ions in the filtrate. Moreover, V (L) denotes the volume of Zn(II), Pb(II), or Cu (II) solution. Additionally, M (g) denotes the mass of the synthesized composite. To investigate the effect of desorption, 50 mg of the synthesized composite were mixed with 80 mL of 5 mg/L of the studied metal ion at pH = 6 for 80 min. Then, filtration was used to separate the solid phase from the liquid phase, which was then washed many times with distilled water

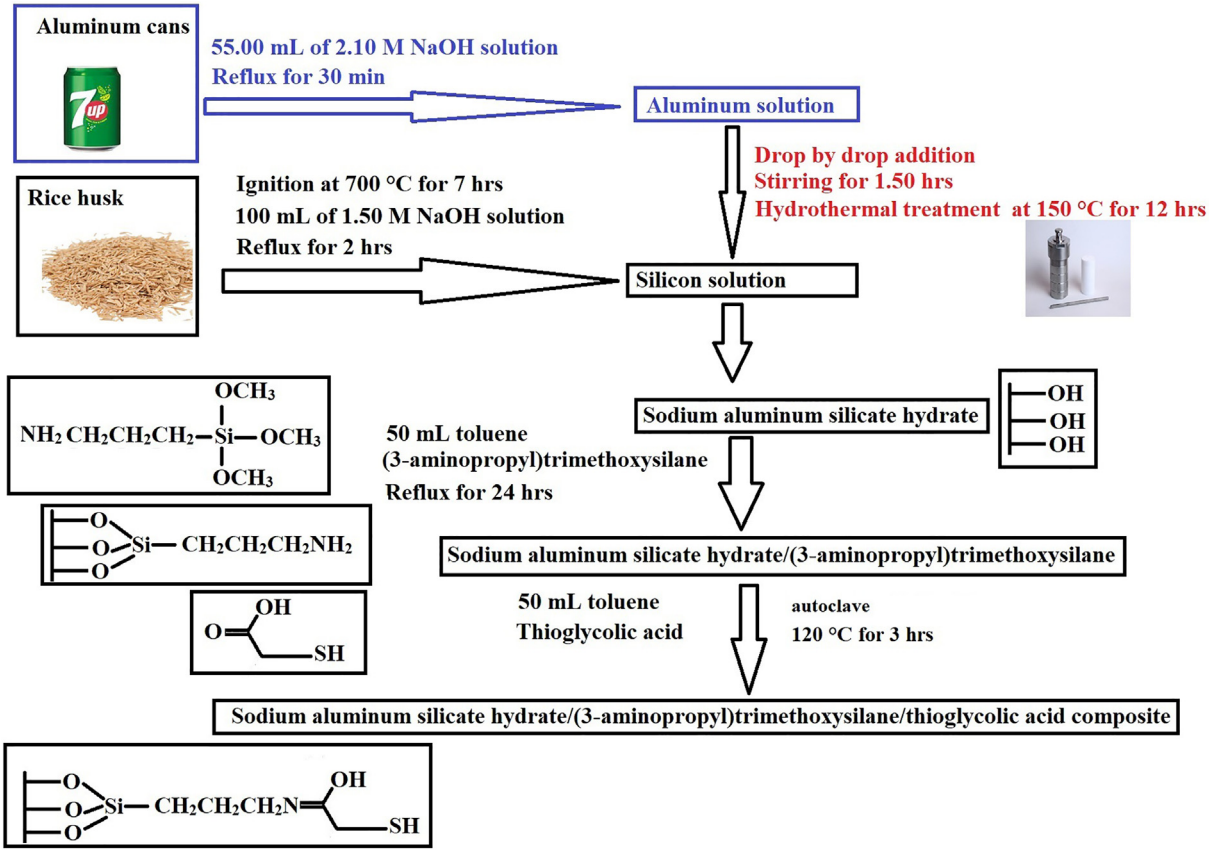

Scheme 1 The synthetic steps of the sodium aluminum silicate hydrate/thioglycolic acid composite.

to remove unloaded ions. Besides, adsorbed ions on the synthesized composite were desorbed by shaking for 10 min with 5 mL of 0.5 M of desorbing agents, for example, thiourea, EDTA disodium salt, and HNO_3. Eq. (3) was utilized to determine the % desorption (% D).

$$\%D = \frac{100 C_d V_d}{(C_i - C_e)V} \tag{3}$$

C_d (mg/L) denotes the concentration of Zn(II), Pb(II), or Cu(II) in the eluate. Besides, V_d (L) denotes the volume of the eluent. Four successive adsorption/desorption runs were accomplished to determine the reusability of the synthesized composite. Following each run, the adsorbent was repeatedly washed carefully with distilled water to prepare it for the following adsorption run. After each run, the percent removal (% R) was calculated using Eq. (1). Khalifa et al. method was used to calculate the point of zero charge (pH_{PZC}) of the synthesized composite (Khalifa et al., 2020) as the following: the initial pH value of 50 mL of 0.025 M KCl solutions was modified to accommodate a range of pH values ranging from 2.00 to 12.00 utilizing 0.1 M HCl or NaOH. Besides, 0.15 g of the synthesized composite was mixed with each KCl solution then the mixture was stirred for 8 hrs. After that, filtration was used to separate the solid phase from the liquid phase then the final pH value (pH_{final}) of the filtrate was determined. The pH_{final} values were plotted versus the $pH_{initial}$ values. The pH_{pzc} value represents the pH_{final} value at which a typical plateau is reached (Khalifa et al., 2020).

2.5. Actual real sample collection and pretreatment

Water samples were gathered from several places in polypropylene flasks which were prewashed using nitric acid (10 % V/V). Before keeping the collected samples in the refrigerator, they were filtered using pore-size membranes (0.45-μm) and acidified to a pH of 2.0 using HNO_3. Food samples (spinach, chicken, and fish) were obtained from the local markets at Benha city, Egypt. Each sample's edible portion was separated and carefully washed using distilled water before being cut into little pieces. Following 12 hrs of drying at 65 °C, the samples were ground until homogeneity was achieved then kept in polyethylene grabs. The samples were digested using a microwave-assisted acid digestion technique for attaining a short-term process. 0.5 g of dry sample was collected in Teflon digesting tubes separately then 2 mL of 30 % H_2O_2 and 4 mL of HNO_3 were added. After 15 min at room temperature, the tubes were hermetically sealed then heated accordance to the one-step procedure outlined below (power: 1650 W; temperature: 200 °C; ramp time: 16 min; cooling time: 16 min; hold time: 16 min). After rewarming the tubes to room temperature, the solutions were almost totally evaporated and then diluted with distilled water to 50 mL.

2.6. Preconcentration process

In a conical flask, 50 mL of digested solution or water sample was combined with 0.05 g of the synthesized composite. The

pH of the solution was changed to 6.0 with NaOH and/or HCl solutions, and the volume of solution was increased to 80 mL using distilled water. Also, the contents were stirred for 80 min then the adsorbent substance was separated and poured into a 25 mL beaker. After adding 5 mL of 0.5 M HNO_3, the mixture was stirred for 10 min to allow the metal ions to desorb. The filtrate was then analyzed for determining the concentration of studied metal ions using atomic absorption spectrometer.

3. Results and discussion

3.1. Characterization of the synthesized composite

Fig. 1A–B illustrate the X-ray diffraction patterns of sodium aluminum silicate hydrate and sodium aluminum silicate hydrate/(3-aminopropyl)trimethoxysilane/thioglycolic acid composite, respectively (Abdelrahman et al., 2021). The distinct peaks of sodium aluminum silicate hydrate at 2θ = 13.9°, 24.3°, 31.6°, 34.7°, 37.4°, 42.8°, 52.0°, 58.2°, 62.0°, and 63.9° correspond to the lattice plans (110), (211), (310), (222), (321), (411), (510), (440), (600), and (611), respectively (Abdelrahman et al., 2021). The XRD pattern of the synthesized composite shows that there is a halo at 2θ = 25.0, which means that there is a crystalline structure that is combined with an amorphous background (Khalifa et al., 2020).

Fig. 2 illustrates the FT-IR spectrum of sodium aluminum silicate hydrate/(3-aminopropyl)trimethoxysilane/thioglycolic acid composite. The peaks, which were observed at 3590 and 1645 cm^{-1}, are attributed to the stretching and bending vibration of adsorbed H_2O and/or C═N, respectively. The peaks, which were observed at 2600 and 2810 cm^{-1}, are attributed to the stretching vibration of SH and CH, respectively. Moreover, the peaks, which were observed at 1475 and 992 cm^{-1}, are attributed to external and internal asymmetric stretching of X-O-X (X = Si and/or Al), respectively. Also, the peaks, which were observed at 710 and 626 cm^{-1}, are attributed to external and internal symmetric stretching of X-O-X ((X = Si and/or Al), respectively. Besides, the peaks, which were observed at 563 and 460 cm^{-1}, are attributed to double ring vibration and bending vibration of X-O-X (X = Si and/or Al), respectively (Abdelrahman et al., 2021; Abdelrahman and Hegazey, 2019a, 2019b; Al-Wasidi et al., 2022b; Khalifa et al., 2020). The elemental analysis of the sodium aluminum silicate hydrate/(3-aminopropyl)trimethoxysilane/thioglycolic acid composite shows carbon, hydrogen, nitrogen, and sulfur content of 15.12, 2.50, 1.41, and 8.50 %, respectively. The SEM and TEM studies indicate that the synthesized composite has a structure similar to that of cotton. Hence, this indicates that the crystalline phase is combined with an amorphous background as shown in Figs. 3 and 4, respectively. The

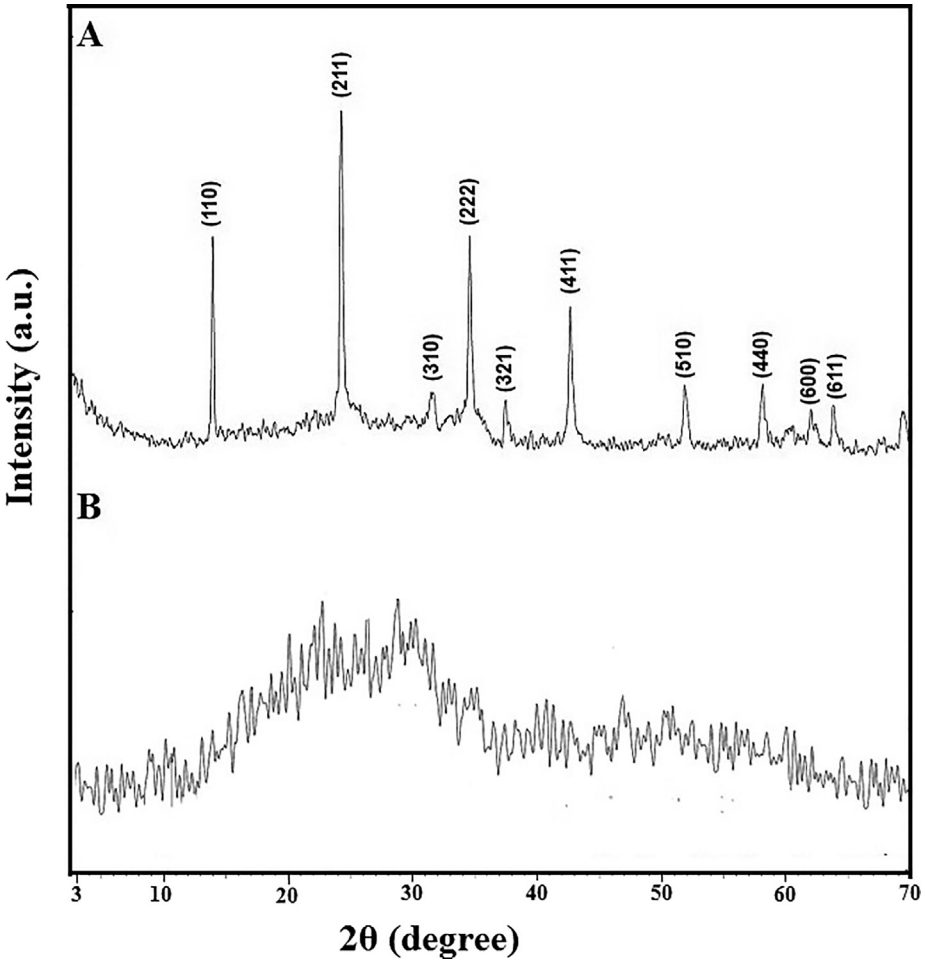

Fig. 1 The X-ray diffraction patterns of the sodium aluminum silicate hydrate (A) and their thioglycolic acid composite (B).

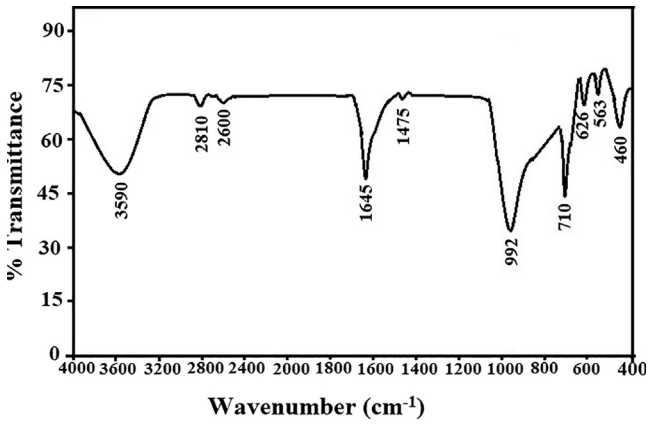

Fig. 2 The FT-IR spectra of the sodium aluminum silicate hydrate/thioglycolic acid composite.

BET study exhibits that the synthesized composite is mesoporous (average pore radius = 4.20 nm) with an average surface area and total pore volume of 3.05 m^2/g and 3.92 × 10^{3-} cc/g, respectively (Abdelrahman and Hegazey, 2019a, 2019b). The anticipated decline in the surface area following functionalization is owing to the presence of organic functional groups on the sodium aluminum silicate hydrate backbone, which prevent nitrogen gas from entering the sodium aluminum silicate hydrate pores during the BET method (Abdelrahman et al., 2021; Abdelrahman and Hegazey, 2019a, 2019b).

3.2. Extraction of Cu(II), Pb(II), and Zn(II) ions from aqueous solutions

3.2.1. Effect of pH

Fig. 5A-B represents the effect of pH on % R of Pb(II), Cu(II), or Zn(II) ions and adsorption capacity of the synthesized composite, respectively. It was found that when the pH is raised from 2 to 6, both the removal percentage and the adsorption capacity go up a lot. Also, it was found that there is a slight increase when the pH changes from 6 to 8 due to the saturation of active sites. As a result, pH = 6 was chosen as the optimal pH for the subsequent studies. % Removal of Pb(II), Cu(II), and Zn(II) ions at pH = 6 is 94.10, 81.62, and 62.08 %, respectively. At pH = 6, the produced composite has an adsorption capacity of 180.67, 156.70, and 119.20 mg/g for Pb(II), Cu(II), and Zn(II) ions, respectively. The pH_{final} vs $pH_{initial}$ curve for several KCl solutions is given in Fig. 5C. Besides, the results indicated that the composite point of zero charge is 3.51. It

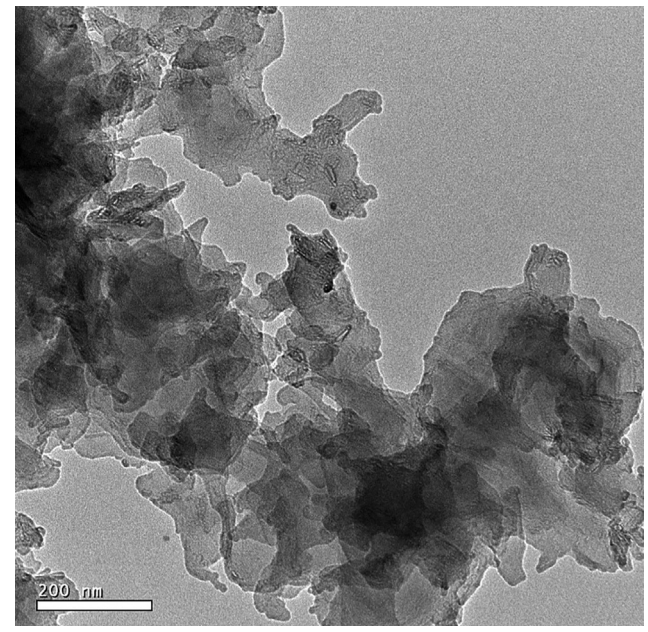

Fig. 4 The HR-TEM image of the sodium aluminum silicate hydrate /thioglycolic acid composite.

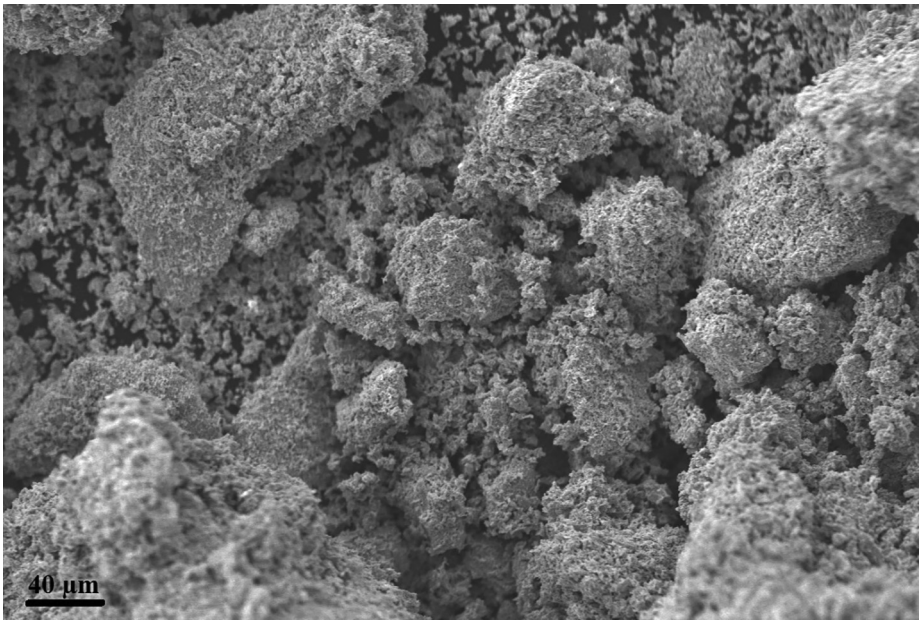

Fig. 3 The FE-SEM image of the sodium aluminum silicate hydrate/thioglycolic acid composite.

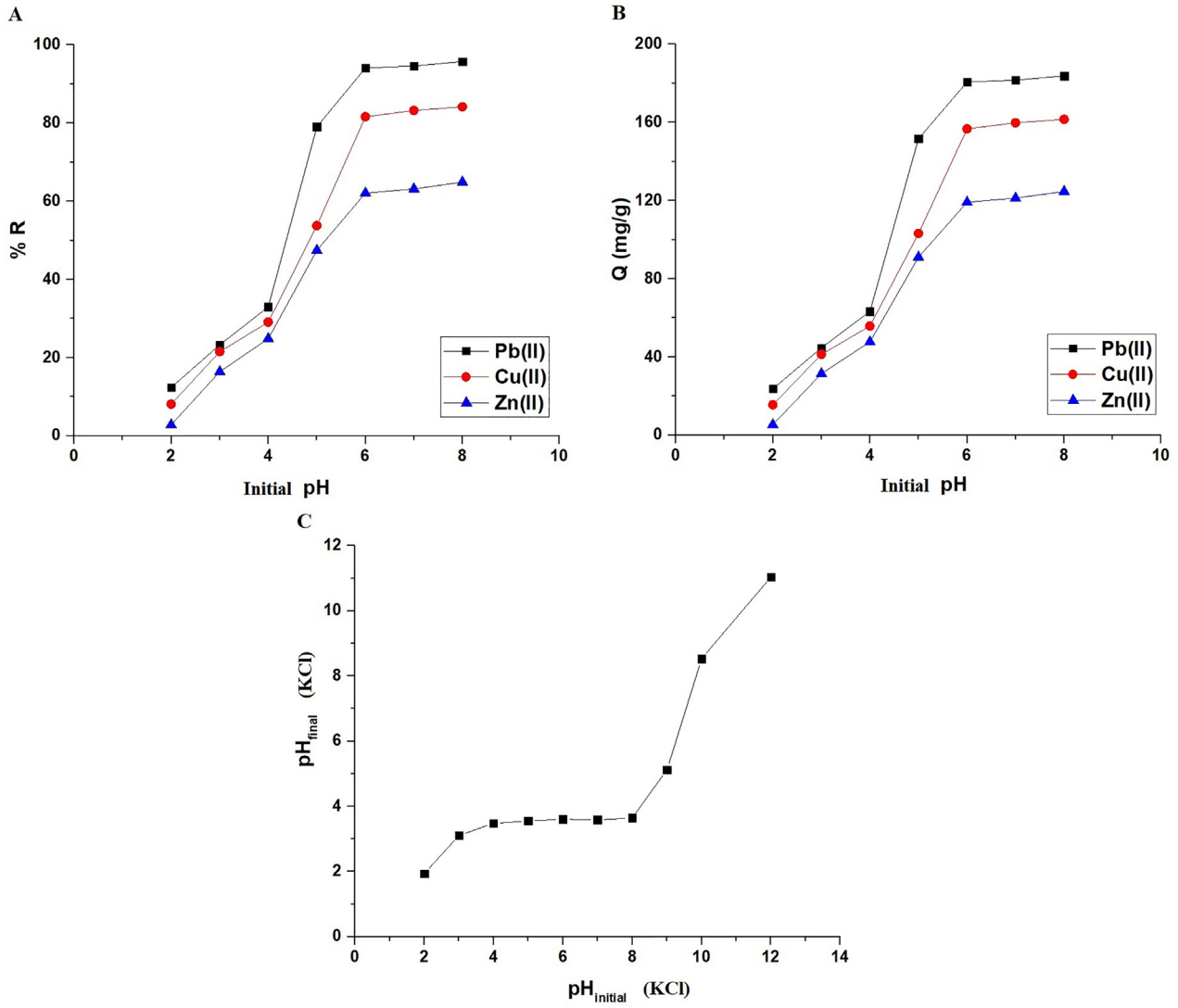

Fig. 5 The influence of pH of the examined metal ion solution on % removal (A) and adsorption capacity (B). Determination of point of zero charge via the plot of pH_{final} versus $pH_{initial}$ for several KCl solutions (C).

was found that when the pH of the Cu(II), Pb(II), or Zn(II) solution is not greater than 3.51, the synthesized composite has a positive charge due to the presence of positive hydrogen ions which repelled the investigated ions, resulting in a reduction in the removal percentage and the adsorption capacity. Also, when the pH of the Cu(II), Pb(II), or Zn(II) solution is greater than 3.51, the synthesized composite has a negative charge due to the presence of negative hydroxide ions which are attracted to the investigated ions and therefore increase the removal percentage and the adsorption capacity (Abdelrahman and Hegazey, 2019a, 2019b; Al-Wasidi et al., 2022b; Khalifa et al., 2020).

3.2.2. Effect of time

Fig. 6A-B represents the effect of time on % R of Pb(II), Cu (II), or Zn(II) ions and adsorption capacity of the synthesized composite, respectively. It was found that when the time is raised from 5 to 80 min, both the removal percentage and the adsorption capacity go up a lot. Also, it was found that there is a slight increase when the time changes from 80 to 120 min owing to the saturation of the active sites. As a result, time = 80 min was chosen as the optimal time for the subsequent studies. % Removal of Pb(II), Cu(II), and Zn(II) ions at time = 80 min is 94.17, 82.50, and 63.33 %, respectively. At time = 80 min, the produced composite has an adsorption capacity of 180.80, 158.40, and 121.60 mg/g toward Pb(II), Cu (II), and Zn(II) ions, respectively. Two kinetic models were employed to investigate the influence of contact time: pseudo-second-order (Eq. (4)) and pseudo-first-order (Eq. (5) (Abdelrahman and Hegazey, 2019a, 2019b; Al-Wasidi et al., 2022b; Khalifa et al., 2020).

$$\frac{t}{Q_t} = \frac{1}{K_2 Q_e^2} + \frac{1}{Q_e} t \tag{4}$$

$$\log (Q_e - Q_t) = log Q_e - \frac{K_1}{2.303} t \tag{5}$$

Q_e (mg/g) is the equilibrium adsorption capacity of the synthesized composite toward the examined metal ions. Q_t (mg/g) denotes the adsorption capacity of the synthesized composite

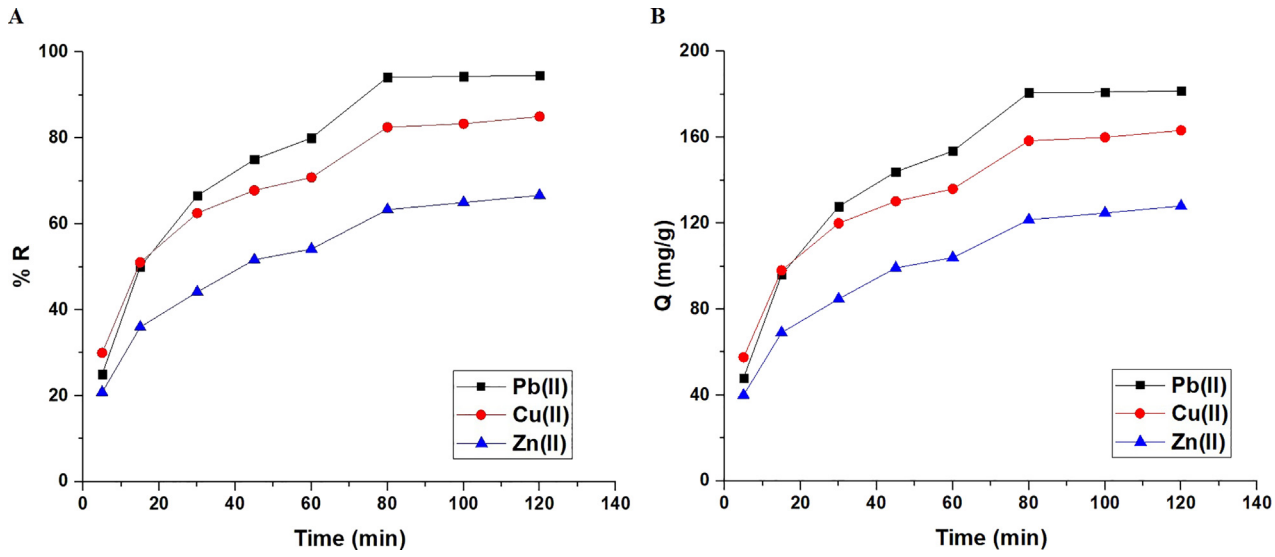

Fig. 6 The influence of contact time of the examined metal ion solution on % removal (A) and adsorption capacity (B).

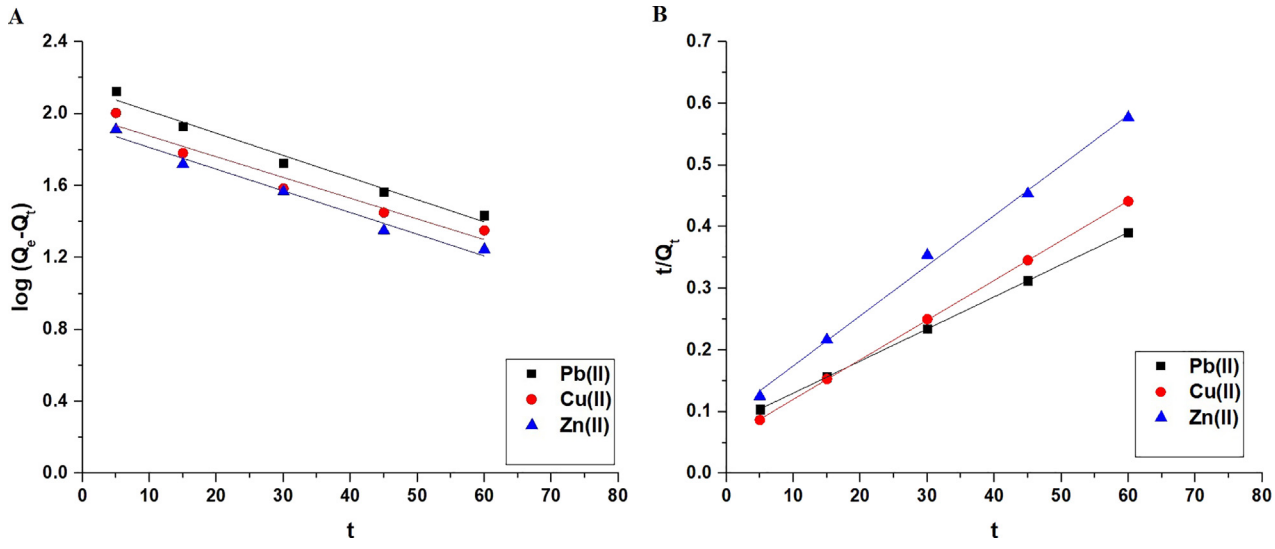

Fig. 7 The pseudo-first-order (A) and pseudo-second-order (B) kinetic models.

Table 1 Kinetic constants for the removal of Pb(II), Cu(II), and Zn(II) ions using the sodium aluminum silicate hydrate /thioglycolic acid composite.

Metal ion	Pseudo first order				Pseudo second order			
	Q_e (mg/g)		K_1 (1/min)	R^2	Q_e (mg/g)		K_2 (g/mg.min)	R^2
	Calculated	Experimental			Calculated	Experimental		
Pb(II)	137.10	180.80	0.0283	0.9723	191.94	180.80	0.00035	0.9999
Cu(II)	97.95	156.70	0.0266	0.9363	155.28	156.70	0.00074	0.9994
Zn(II)	85.63	119.20	0.0278	0.9749	123.15	119.20	0.00071	0.9958

toward the metal ions under investigation at the contact time t. The pseudo-first-order model's rate constant is denoted by K_1 (1/min), whereas the pseudo-second-order model's rate constant is denoted by K_2 (g/mg.min). Fig. 7A-B illustrate the pseudo-first-order and pseudo-second-order models, respectively. The correlation coefficients (R^2) of the pseudo-first-order model are smaller than those of the pseudo-second-order model, as shown in Table 1. Additionally, the

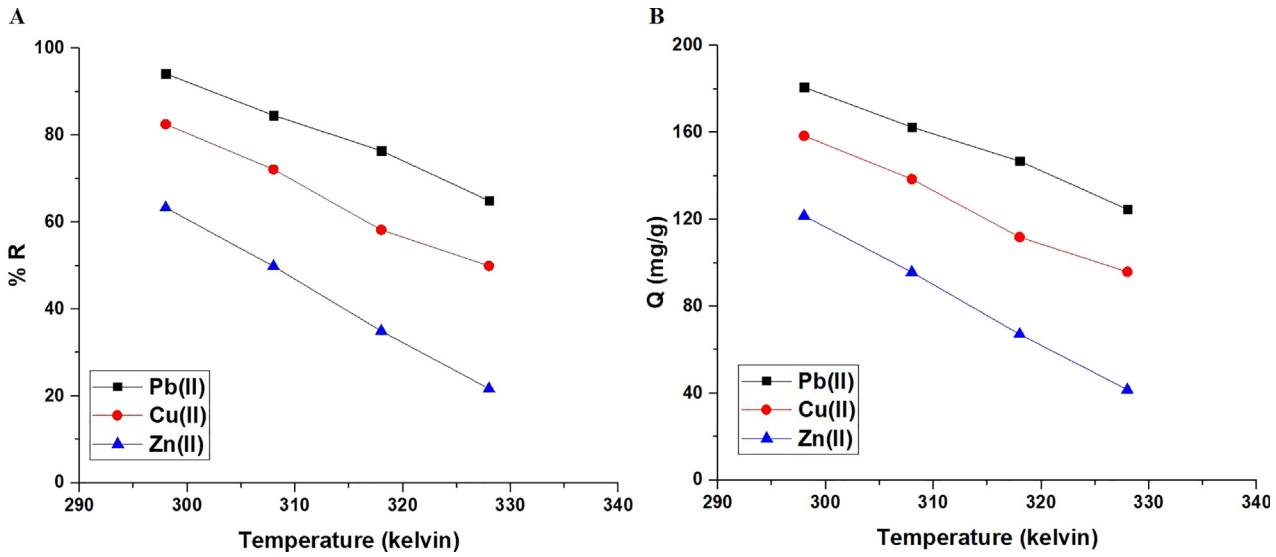

Fig. 8 The influence of temperature of the examined metal ion solution on % removal (A) and adsorption capacity (B).

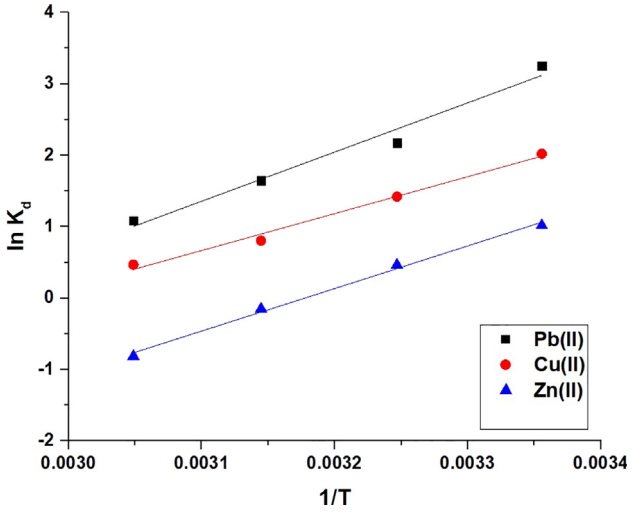

Fig. 9 The plot of $\ln K_d$ versus temperature.

pseudo-second-order adsorption capacity is more consistent with experimental adsorption capacity than that of the pseudo-first-order. Consequently, the pseudo-second-order model explained the kinetic data more accurately than the pseudo-first-order model. Thus, the chemical reaction appears to be involved in the rate-controlling step.

3.2.3. *Effect of temperature*

Fig. 8A-B represents the effect of temperature on % R of Pb (II), Cu(II), or Zn(II) ions and adsorption capacity of the synthesized composite, respectively. It was found that when the temperature is raised from 298 to 328 K, both the removal percentage and the adsorption capacity decrease. As a result, temperature = 298 K was chosen as the optimal temperature for the subsequent studies. % Removal of Pb(II), Cu(II), and Zn(II) ions at temperature = 328 K is 64.90, 49.94, and 21.70 %, respectively. At 328 K, the produced composite has an adsorption capacity of 124.61, 95.89, and 41.66 mg/g toward Pb(II), Cu(II), and Zn(II) ions, respectively. The thermodynamic parameters: change in enthalpy (ΔH^o), change in entropy (ΔS^o), and change in free energy (ΔG^o) were calculated using Eqs. (6) & (7) (Abdelrahman and Hegazey, 2019a, 2019b; Al-Wasidi et al., 2022b; Khalifa et al., 2020).

$$lnK_d = \frac{\Delta S^\circ}{R} - \frac{\Delta H^\circ}{RT} \tag{6}$$

$$\Delta G^\circ = \Delta H^\circ - T\Delta S^\circ \tag{7}$$

T (Kelvin) is the adsorption temperature while K_d (L/g) denotes the distribution constant. Additionally, R (kJ/mol kelvin) is a gas constant. The distribution constant was determined using Eq. (8) (Abdelrahman and Hegazey, 2019a, 2019b; Al-Wasidi et al., 2022b; Khalifa et al., 2020).

$$K_d = \frac{Q_e}{C_e} \tag{8}$$

Fig. 9 depicts the $\ln K_d$ versus temperature graph. The thermodynamic parameters are listed in Table 2. Due to the fact that the enthalpy value exceeds 40 kJ/mol, the data established that the adsorption of Cu(II), Pb(II), or Zn(II) ions via the synthesized composite is chemical (Abdelrahman and Hegazey, 2019a, 2019b; Al-Wasidi et al., 2022b; Khalifa et al., 2020). Additionally, due to the negative sign of ΔH^o, the adsorption of Cu(II), Pb(II), or Zn(II) ions is exothermic when the synthesized composite is used (Abdelrahman and Hegazey, 2019a, 2019b; Al-Wasidi et al., 2022b; Khalifa et al., 2020). Moreover, due to the negative sign of the ΔG^o, the adsorption of Cu(II), Pb(II), or Zn(II) ions is spontaneous when using the synthesized composite. Due to the positive sign of ΔS^o, the adsorption of Cu(II), Pb(II), or Zn(II) ions occurs in a disorderly manner at the solution boundary/composite (Abdelrahman and Hegazey, 2019a, 2019b; Al-Wasidi et al., 2022b; Khalifa et al., 2020).

3.2.4. *Effect of concentration*

Fig. 10A–B represents the effect of concentration on % R of Pb(II), Cu(II), or Zn(II) ions and adsorption capacity of the

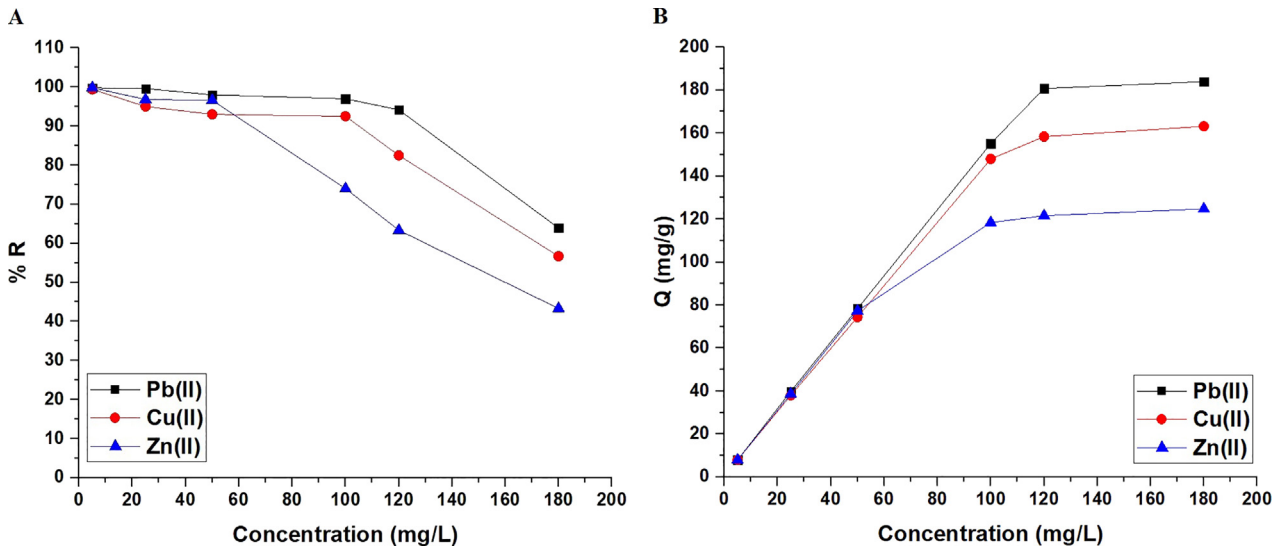

Fig. 10 The influence of concentration of the examined metal ion solution on % removal (A) and adsorption capacity (B).

Table 2 Thermodynamic parameters for the removal of Pb(II), Cu(II), and Zn(II) ions using the sodium aluminum silicate hydrate/thioglycolic acid composite.

Metal ion	ΔG° (KJ/mol)				ΔS° (KJ/molK)	ΔH° (KJ/mol)
	Temperature (kelvin)					
	298	308	318	328		
Pb(II)	−107.55	−109.22	−110.89	−112.57	0.1674	−57.66
Cu(II)	−81.50	−82.79	−84.07	−85.36	0.1284	−43.23
Zn(II)	−96.94	−98.52	−100.11	−101.69	0.1582	−49.79

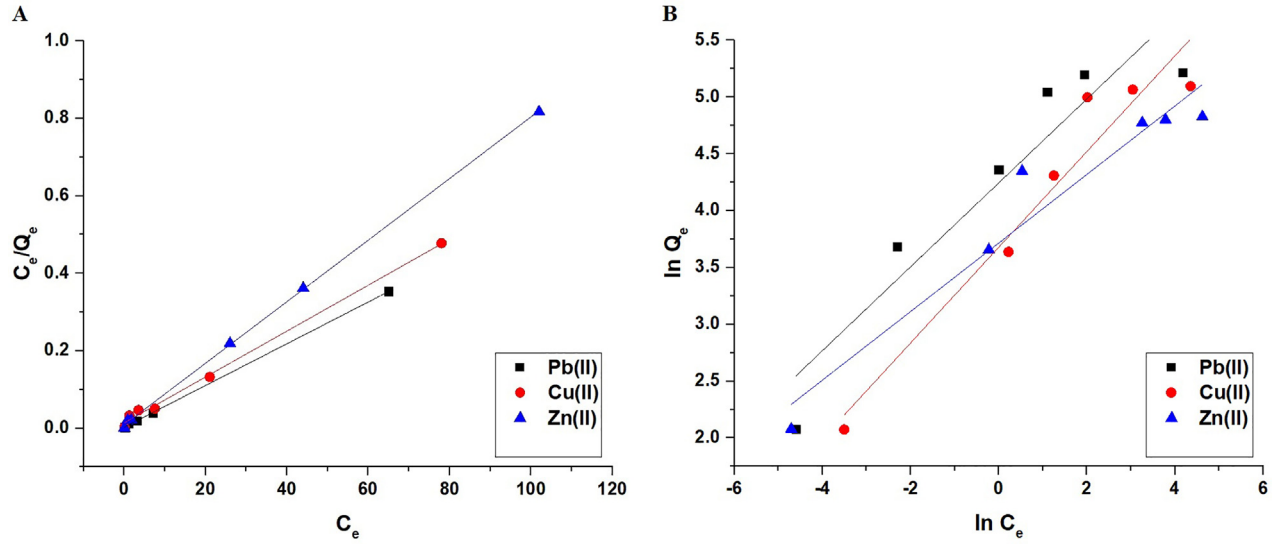

Fig. 11 The Langmuir (A) and Freundlich (B) isotherms.

synthesized composite, respectively. It was found that when the concentration is raised from 5 to 180 mg/L, the removal percentage decreases while the adsorption capacity increases (Abdelrahman and Hegazey, 2019a, 2019b; Al-Wasidi et al., 2022b; Khalifa et al., 2020). Freundlich (Eq. (9)) and Langmuir (Eq. (10)) equilibrium isotherms were utilized for

Table 3 Equilibrium constants for the removal of Pb(II), Cu(II), and Zn(II) ions using the sodium aluminum silicate hydrate / thioglycolic acid composite.

Metal ion	Langmuir			Freundlich		
	Q_m (mg/g)	K_3 (L/mg)	R^2	Q_m (mg/g)	K_4 (mg/g)(L/mg)$^{1/n}$	R^2
Pb(II)	185.53	1.8148	0.9996	407.81	69.7139	0.8581
Cu(II)	168.92	0.4134	0.9962	297.02	39.5679	0.9196
Zn(II)	125.94	0.8429	0.9997	173.99	41.0762	0.9228

Table 4 Comparison of adsorption capacity of various adsorbents toward Pb(II), Cu(II), and Zn(II) ions.

Adsorbent	**Q (mg/g) toward Pb(II) ions**	**Q (mg/g) toward Cu(II) ions**	**Q (mg/g) toward Zn(II) ions**	**Ref**
Xanthate modified magnetic chitosan	76.90	34.50	20.80	Zhu et al., 2012
Cross-linked chitosan with epichlorohydrin	34.13	35.46	10.21	Chen et al., 2008
Iron oxide/activated carbon composite	–	8.06	–	Jain et al., 2018
Zeolite	109.89	57.80	36.77	Joseph et al., 2020
Amidoxime-functionalized polypropylene fiber	45.64	47.23	37.78	Zhao et al., 2020
Maghemite nanotubes	71.42	111.11	84.95	Roy and Bhattacharya, 2012
Carbon gel	16.95	6.64	–	Osińska, 2017
Guanyl-modified cellulose	52.00	83.00	78.00	Kenawy et al., 2018
Sodium aluminum silicate hydrate/(3-aminopropyl) trimethoxysilane/thioglycolic acid composite	185.53	168.92	125.94	**This study**

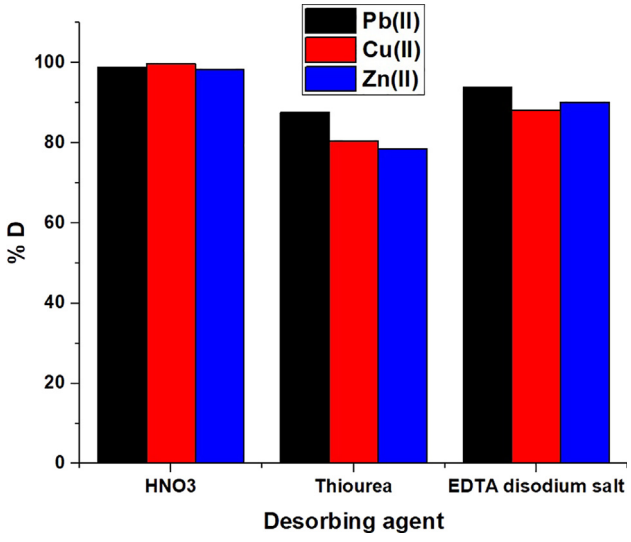

Fig. 12 The plot of % desorption versus several desorbing solutions.

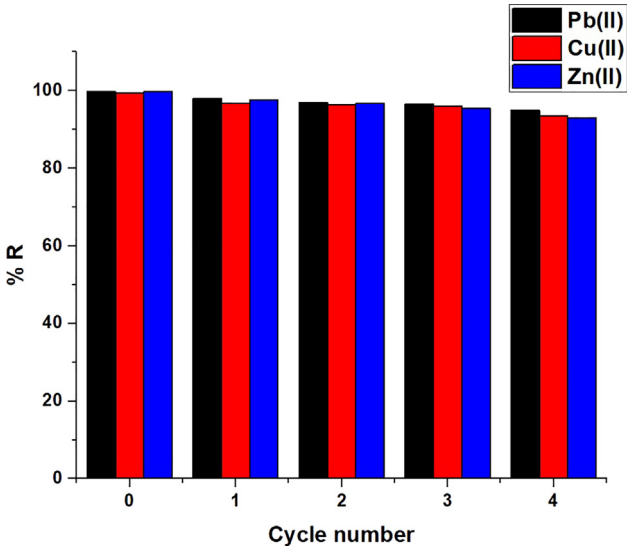

Fig. 13 The plot of % removal versus the cycle number.

analyzing the concentration data (Abdelrahman and Hegazey, 2019a, 2019b; Al-Wasidi et al., 2022b; Khalifa et al., 2020).

$$lnQ_e = lnK_3 + \frac{1}{n} lnC_e \tag{9}$$

$$\frac{C_e}{Q_e} = \frac{1}{K_4 Q_m} + \frac{C_e}{Q_m} \tag{10}$$

Q_m (mg/g) is the maximal adsorption capacity of the synthesized composite. K_4 (L/mg) is the Langmuir constant, while K_3 (mg/g)(L/mg)$^{1/n}$ is the Freundlich constant. 1/n denotes the heterogeneity constant. The Freundlich isotherm can be used to determine the Q_m using Eq. (11) (Abdelrahman and Hegazey, 2019a, 2019b; Al-Wasidi et al., 2022b; Khalifa et al., 2020).

$$Q_m = K_3\left(C_i^{1/n}\right) \tag{11}$$

Table 5 Removal of Pb(II), Cu(II), and Zn(II) ions from binary mixtures in the presence of several diverse ions.

Diverse ion	Tolerance limit (mg/L)	% R		
		Pb(II)	Cu(II)	Zn(II)
K(I)	1000	99.19	99.27	99.23
Na(I)	1000	98.25	99.54	99.16
Ca(II)	100	95.78	95.30	96.05
Ba(II)	80	96.17	97.18	97.07
Mg(II)	100	97.35	98.45	96.43
Hg(II)	80	96.06	96.45	95.87
Cd(II)	80	95.89	96.26	95.90
Fe(II)	100	97.08	97.83	96.32
Mn(II)	100	97.32	95.62	98.11
Ni(II)	100	96.59	97.07	95.85
Al(III)	100	98.26	98.57	97.24
Fe(III)	80	97.84	95.80	96.73
HCO^{3-}	1000	99.57	99.62	99.31
NO^{3-}	1000	99.69	99.48	99.20
Cl^{-}	1000	99.31	99.58	99.60
SO_4^{2-}	1000	99.65	99.90	99.65

Table 6 Results for the calculation of Pb(II) ions in real samples (mean ± (SD × t/$\sqrt{n}$), n = 5, t = 2.776, Confidence level = 95 %).

Sample	Added volume from Pb(II) stock solution (1000 mg/L)								
	0 mL			0.2 mL			0.4 mL		
	Found concentration (mg/L)	% Recovery	% RSD	Found concentration (mg/L)	% Recovery	% RSD	Found concentration (mg/L)	% Recovery	% RSD
Sea water	10.432 ± 0.044	–	0.342	12.862 ± 0.407	99.707	2.552	15.176 ± 0.259	98.830	1.376
River water	7.250 ± 0.248	–	2.759	9.592 ± 0.116	98.625	0.976	12.182 ± 0.194	99.942	1.280
Chicken muscles	8.610 ± 0.198	–	1.855	10.936 ± 0.213	98.679	1.570	13.318 ± 0.299	98.344	1.813
Fish muscles	7.030 ± 0.121	–	1.386	9.220 ± 0.283	96.989	2.473	11.818 ± 0.255	98.729	1.737
Spinach leaves	0.496 ± 0.014	–	2.299	2.87 ± 0.104	96.034	2.915	5.29 ± 0.178	96.733	2.707

Table 7 Results for the calculation of Cu(II) ions in real samples (mean ± (SD × t/$\sqrt{n}$), n = 5, t = 2.776, Confidence level = 95 %).

Sample	Added volume from Zn(II) stock solution (1000 mg/L)								
	0 mL			0.5 mL			1.0 mL		
	Found concentration (mg/L)	% Recovery	% RSD	Found concentration (mg/L)	% Recovery	% RSD	Found concentration (mg/L)	% Recovery	% RSD
Sea water	12.926 ± 0.189	–	1.183	15.314 ± 0.235	99.522	1.239	17.716 ± 0.385	99.322	1.751
River water	10.124 ± 0.172	–	1.366	12.366 ± 0.277	98.201	1.802	14.724 ± 0.303	97.842	1.658
Chicken muscles	39.504 ± 0.692	–	1.412	44.940 ± 0.723	98.835	1.296	50.950 ± 0.328	99.198	0.519
Fish muscles	45.330 ± 0.528	–	0.938	51.200 ± 1.039	99.884	1.634	56.934 ± 0.897	99.681	1.269
Spinach leaves	19.88 ± 0.296	–	1.201	25.660 ± 0.286	98.815	0.897	31.260 ± 0.606	97.748	1.561

Table 8 Results for the calculation of Zn(II) ions in real samples (mean ± (SD × t/√n), n = 5, t = 2.776, Confidence level = 95 %).

Sample	Added volume from Cu(II) stock solution (1000 mg/L)								
	0 mL			0.2 mL			0.4 mL		
	Found concentration (mg/L)	% Recovery	% RSD	Found concentration (mg/L)	% Recovery	% RSD	Found concentration (mg/L)	% Recovery	% RSD
Sea water	4.586 ± 0.159	–	2.799	6.990 ± 0.188	98.892	2.169	9.536 ± 0.144	99.976	1.218
River water	8.970 ± 0.136	–	1.221	11.380 ± 0.143	99.463	1.012	13.720 ± 0.239	98.702	1.402
Chicken muscles	5.958 ± 0.155	–	2.098	8.300 ± 0.133	98.377	1.289	10.838 ± 0.143	99.399	1.061
Fish muscles	8.132 ± 0.162	–	1.609	10.468 ± 0.148	98.704	1.135	12.844 ± 0.121	98.296	0.756
Spinach leaves	6.956 ± 0.072	–	0.829	9.426 ± 0.156	99.932	1.337	11.802 ± 0.176	99.206	1.202

Fig. 11A–B illustrate the Langmuir and Freundlich isotherms, respectively. As indicated in Table 3, the Freundlich isotherm correlation coefficients (R^2) are less than those of Langmuir. Accordingly, the Langmuir isotherm performed better than the Freundlich isotherm in representing equilibrium data. The synthesized composite has a maximum absorption capacity of 185.53, 168.92, and 125.94 mg/g for Pb(II), Cu(II), and Zn(II) ions, respectively. Besides, as illustrated in Table 4, the synthetic composite's adsorption capability was compared to that of various adsorbents such as xanthate modified magnetic chitosan, cross-linked chitosan with epichlorohydrin, iron oxide/activated carbon composite, zeolite, amidoxime-functionalized polypropylene fiber, maghemite nanotubes, carbon gel, and guanyl-modified cellulose (Chen et al., 2008; Jain et al., 2018; Joseph et al., 2020; Kenawy et al., 2018; Osińska, 2017; Roy and Bhattacharya, 2012; Zhao et al., 2020; Zhu et al., 2012). The synthesized composite outperformed the majority of adsorbents due to its high adsorption capacity.

3.2.5. *Effect of desorption and reusability*

The plot of % desorption versus some desorbing agents is presented in Fig. 12. Desorbing agents included 0.5 M EDTA disodium salt, nitric acid, and thiourea. The results indicate that 0.5 M of nitric acid is the optimal desorbing agent for retrieving the maximum amount of studied ions from the synthesized composite. Moreover, the plot of % removal versus the cycle number is presented in Fig. 13. The slight drop in percent removal indicates that the produced composite can be efficiently regenerated and reutilized for the adsorption of Cu(II), Pb(II), and Zn(II) ions from aqueous media.

3.2.6. *Effect of co-existing ions*

To investigate the influence of several anions and cations on the extraction efficacy of Cu(II), Pb(II), and Zn(II) ions operating the present process, the potential interfering ion was added at various concentrations to a 80 mL solution containing 220 µg/L of the examined metal ion individually. The extraction procedure was carried out exactly as stated previously, and the extraction efficacy was assessed. The tolerance limit was determined as the greatest concentration of the accompanying ion that produced a 5 % mistake through the extraction procedure. Table 5 obviously demonstrates that the majority of coexisting ions have a reasonably high tolerance limit, showing the procedure's selectivity. As a result, the approach can be used for analyzing real samples of varied components.

3.3. *Application*

The proposed separation procedure was used to preconcentrate Cu(II), Pb(II), and Zn(II) in real samples (Sea water, river water, fish muscles, chicken muscles, and spinach leaves) prior to atomic absorption spectrometer analysis. Tables 6, 7, and 8 summarizes the results of preconcentration of Cu(II), Pb(II), and Zn(II) ions along with the recoveries for the spiked samples, respectively. The recovery findings demonstrate that the process is accurate, adaptable, and resulted in quantitative separation (greater than95 percent). Furthermore, the % RSD was less than 3.5 percent, indicating good reproducibility.

4. Conclusions

In the current study, sodium aluminum silicate hydrate was prepared and chemically modified using thioglycolic acid with the assistance of microwave radiation. The synthesized composite was characterized using some physical and chemical devices and was employed for the removal and preconcentration of Cu(II), Pb(II), and Zn(II) ions from aqueous solutions and food samples (Sea water, river water, fish muscles, chicken muscles, and spinach leaves). The thermodynamic experiments revealed an exothermic, chemical, and spontaneous adsorption process. Commonly occurring interfering ions had no effect on the removal process. The composite can be used for at least four adsorption/desorption cycles without losing adsorption effectiveness. The synthesized composite has a maximum absorption capacity of 168.92, 185.53, and 125.94 mg/g for Cu(II), Pb(II), and Zn(II) ions, respectively.

Declaration of Competing Interest

The authors declare that they have no known competing financial interests or personal relationships that could have appeared to influence the work reported in this paper.

Acknowledgements

The authors are grateful to Princess Nourah Bint Abdulrahman University, Riyadh, Saudi Arabia for funding this work through Researchers Supporting Project number (PNURSP2022R35).

References

Abdelrahman, E.A., 2018. Synthesis of zeolite nanostructures from waste aluminum cans for efficient removal of malachite green dye from aqueous media. J. Mol. Liq. 253, 72–82. https://doi.org/10.1016/j.molliq.2018.01.038.

Abdelrahman, E.A., Abou El-Reash, Y.G., Youssef, H.M., Kotp, Y. H., Hegazey, R.M., 2021. Utilization of rice husk and waste aluminum cans for the synthesis of some nanosized zeolite, zeolite/zeolite, and geopolymer/zeolite products for the efficient removal of Co(II), Cu(II), and Zn(II) ions from aqueous media. J. Hazard. Mater. 401,. https://doi.org/10.1016/j.jhazmat.2020.123813 123813.

Abdelrahman, E.A., Hegazey, R.M., 2019a. Utilization of waste aluminum cans in the fabrication of hydroxysodalite nanoparticles and their chitosan biopolymer composites for the removal of Ni(II) and Pb(II) ions from aqueous solutions: Kinetic, equilibrium, and reusability studies. Microchem. J. 145, 18–25. https://doi.org/10.1016/j.microc.2018.10.016.

Abdelrahman, E.A., Hegazey, R.M., 2019b. Exploitation of Egyptian insecticide cans in the fabrication of Si / Fe nanostructures and their chitosan polymer composites for the removal of Ni (II), Cu (II), and Zn (II) ions from aqueous solutions. Compos. Part B 166, 382–400. https://doi.org/10.1016/j.compositesb.2019.02.027.

Ahmad, H., Huang, Z., Kanagaraj, P., Liu, C., 2020. Separation and preconcentration of arsenite and other heavy metal ions using graphene oxide laminated with protein molecules. J. Hazard. Mater. 384,. https://doi.org/10.1016/j.jhazmat.2019.121479 121479.

Akhtar, M., Iqbal, S., Kausar, A., Bhanger, M.I., Shaheen, M.A., 2010. An economically viable method for the removal of selected divalent metal ions from aqueous solutions using activated rice husk. Colloids Surfaces B Biointerfaces 75, 149–155. https://doi.org/10.1016/j.colsurfb.2009.08.025.

Al-wasidi, A.S., Alsalem, H.S., Alshalawi, A.F., Naglah, A.M., Al-anwar, A., Abdelrahman, E.A., 2022. Facile synthesis of a novel nanocomposite for determination of mercury and copper ions in food and water samples. Arab. J. Chem. 15,. https://doi.org/10.1016/j.arabjc.2022.104113 104113.

Al-Wasidi, A.S., Naglah, A.M., Saad, F.A., Abdelrahman, E.A., 2022a. Modification of silica nanoparticles with 1-hydroxy-2-acetonaphthone as a novel composite for the efficient removal of Ni(II), Cu(II), Zn(II), and Hg(II) ions from aqueous media. Arab. J. Chem. 15,. https://doi.org/10.1016/j.arabjc.2022.104010 104010.

Al-Wasidi, A.S., Naglah, A.M., Saad, F.A., Abdelrahman, E.A., 2022b. Modification of Silica Nanoparticles with 4,6-Diacetylresorcinol as a Novel Composite for the Efficient Removal of Pb(II), Cu(II), Co(II), and Ni(II) Ions from Aqueous Media. J. Inorg. Organomet. Polym. Mater. https://doi.org/10.1007/s10904-022-02282-4.

Chen, S.H., Li, Y.X., Li, P.H., Xiao, X.Y., Jiang, M., Li, S.S., Zhou, W.Y., Yang, M., Huang, X.J., Liu, W.Q., 2018. Electrochemical spectral methods for trace detection of heavy metals: A review. TrAC - Trends Anal. Chem. 106, 139–150. https://doi.org/10.1016/j.trac.2018.07.005.

Chen, A.H., Liu, S.C., Chen, C.Y., Chen, C.Y., 2008. Comparative adsorption of Cu(II), Zn(II), and Pb(II) ions in aqueous solution on the crosslinked chitosan with epichlorohydrin. J. Hazard. Mater. 154, 184–191. https://doi.org/10.1016/j.jhazmat.2007.10.009.

Covre, W.P., Ramos, S.J., Pereira, W.V. da S., Souza, E.S. de, Martins, G.C., Teixeira, O.M.M., Amarante, C.B. do, Dias, Y.N., Fernandes, A.R., 2022. Impact of copper mining wastes in the Amazon: Properties and risks to environment and human health. J. Hazard. Mater. 421. https://doi.org/10.1016/j.jhazmat.2021.126688.

Dai, Y., Sun, Q., Wang, W., Lu, L., Liu, M., Li, J., Yang, S., Sun, Y., Zhang, K., Xu, J., Zheng, W., Hu, Z., Yang, Y., Gao, Y., Chen, Y., Zhang, X., Gao, F., Zhang, Y., 2018. Utilizations of agricultural waste as adsorbent for the removal of contaminants: A review. Chemosphere 211, 235–253. https://doi.org/10.1016/j.chemosphere.2018.06.179.

Disilvestro, R.A., Joseph, E.L., Zhang, W., Raimo, A.E., Kim, Y.M., 2012. A randomized trial of copper supplementation effects on blood copper enzyme activities and parameters related to cardiovascular health. Metabolism. 61, 1242–1246. https://doi.org/10.1016/j.metabol.2012.02.002.

El-Shafey, E.I., 2010. Removal of Zn(II) and Hg(II) from aqueous solution on a carbonaceous sorbent chemically prepared from rice husk. J. Hazard. Mater. 175, 319–327. https://doi.org/10.1016/j.jhazmat.2009.10.006.

Hussain, T., Hussain, M., Hussain, S., Kaseem, M., 2022. Microwave-assisted synthesis of NiTe2 photocatalyst as a facile and scalable approach for energy-efficient photocatalysis and detoxification of harmful organic dyes. Sep. Purif. Technol. 282,. https://doi.org/10.1016/j.seppur.2021.120025 120025.

Iqbal, A., Jan, M.R., Shah, J., Rashid, B., 2020. Dispersive solid phase extraction of precious metal ions from electronic wastes using magnetic multiwalled carbon nanotubes composite. Miner. Eng. 154,. https://doi.org/10.1016/j.mineng.2020.106414 106414.

Jain, M., Yadav, M., Kohout, T., Lahtinen, M., Garg, V.K., Sillanpää, M., 2018. Development of iron oxide/activated carbon nanoparticle composite for the removal of Cr(VI), Cu(II) and Cd(II) ions from aqueous solution. Water Resour. Ind. 20, 54–74. https://doi.org/10.1016/j.wri.2018.10.001.

Joseph, I.V., Tosheva, L., Doyle, A.M., 2020. Simultaneous removal of Cd(II), Co(II), Cu(II), Pb(II), and Zn(II) ions from aqueous solutions via adsorption on FAU-type zeolites prepared from coal fly ash. J. Environ. Chem. Eng. 8,. https://doi.org/10.1016/j.jece.2020.103895 103895.

Kamari, S., Ghorbani, F., 2021. Extraction of highly pure silica from rice husk as an agricultural by-product and its application in the production of magnetic mesoporous silica MCM–41. Biomass Convers. Biorefinery 11, 3001–3009. https://doi.org/10.1007/s13399-020-00637-w.

Kenawy, I.M., Hafez, M.A.H., Ismail, M.A., Hashem, M.A., 2018. Adsorption of Cu(II), Cd(II), Hg(II), Pb(II) and Zn(II) from aqueous single metal solutions by guanyl-modified cellulose. Int. J. Biol. Macromol. 107, 1538–1549. https://doi.org/10.1016/j.ijbiomac.2017.10.017.

Khalifa, M.E., Abdelrahman, E.A., Hassanien, M.M., Ibrahim, W.A., 2020. Application of Mesoporous Silica Nanoparticles Modified with Dibenzoylmethane as a Novel Composite for Efficient Removal of Cd(II), Hg(II), and Cu(II) Ions from Aqueous Media. J. Inorg. Organomet. Polym. Mater. 30, 2182–2196. https://doi.org/10.1007/s10904-019-01384-w.

Li, X., Zhou, Y., Zhang, J., 2021. Status and associated human health risk of zinc accumulation in agricultural soils across China. Process Saf. Environ. Prot. 146, 867–876. https://doi.org/10.1016/j.psep.2020.12.017.

Liu, H., Zhao, Y., Zhou, C., Mu, B., Chen, L., 2021. Microwave-assisted synthesis of Zr-based metal–organic framework (Zr-fum-fcu-MOF) for gas adsorption separation. Chem. Phys. Lett. 780,. https://doi.org/10.1016/j.cplett.2021.138906 138906.

Mandal, S., Lahiri, S., 2022. A review on extraction, preconcentration and speciation of metal ions by sustainable cloud point extraction. Microchem. J. 175,. https://doi.org/10.1016/j.microc.2021.107150 107150.

Naeimi, A., Sharifi, A., Abhari, A.R., Farrokhzadeh, S., Jannat, B., 2022. Crystalline phase formation of Na2W2O7 using microwave-assisted solution combustion synthesis for photocatalytic degradation of organic pollutants from aqueous solutions. J. Mol. Struct. 1250,. https://doi.org/10.1016/j.molstruc.2021.131696 131696.

Osińska, M., 2017. Removal of lead(II), copper(II), cobalt(II) and nickel(II) ions from aqueous solutions using carbon gels. J. Sol-Gel Sci. Technol. 81, 678–692. https://doi.org/10.1007/s10971-016-4256-0.

Ramezani, A.M., Ahmadi, R., Yamini, Y., 2022. Homogeneous liquid-liquid microextraction based on deep eutectic solvents. TrAC - Trends Anal. Chem. 149,. https://doi.org/10.1016/j.trac.2022.116566 116566.

Rani, I., Goyal, A., Bhatnagar, M., Manhas, S., Goel, P., Pal, A., Prasad, R., 2021. Potential molecular mechanisms of zinc- and copper-mediated antiviral activity on COVID-19. Nutr. Res. 92, 109–128. https://doi.org/10.1016/j.nutres.2021.05.008.

Roy, A., Bhattacharya, J., 2012. Removal of Cu(II), Zn(II) and Pb(II) from water using microwave-assisted synthesized maghemite nanotubes. Chem. Eng. J. 211–212, 493–500. https://doi.org/10.1016/j.cej.2012.09.097.

Saeed, A.H.A., Yub Harun, N., Mahmoud Nasef, M., Al-Fakih, A., Ghaleb, A.A.S., Kolawole Afolabi, H., 2022. Removal of cadmium from aqueous solution by optimized rice husk biochar using response surface methodology. Ain Shams Eng. J. 13. https://doi.org/10.1016/j.asej.2021.06.002.

Seliem, M.K., Komarneni, S., Abu Khadra, M.R., 2016. Phosphate removal from solution by composite of MCM-41 silica with rice husk: Kinetic and equilibrium studies. Microporous Mesoporous Mater. 224, 51–57. https://doi.org/10.1016/j.micromeso.2015.11.011.

Słota, M., Wąsik, M., Stołtny, T., Machoń-Grecka, A., Kasperczyk, S., 2022. Effects of environmental and occupational lead toxicity and its association with iron metabolism. Toxicol. Appl. Pharmacol. 434. https://doi.org/10.1016/j.taap.2021.115794.

Takahashi, A., 2022. Role of Zinc and Copper in Erythropoiesis in Patients on Hemodialysis. J. Ren. Nutr. https://doi.org/10.1053/j.jrn.2022.02.007.

Wang, Z., Yu, C., Huang, H., Guo, W., Yu, J., Qiu, J., 2021. Carbon-enabled microwave chemistry: From interaction mechanisms to nanomaterial manufacturing. Nano Energy 85,. https://doi.org/10.1016/j.nanoen.2021.106027 106027.

Xiong, Y., Cui, X., Wang, D., Wang, Y., Lou, Z., Shan, W., Fan, Y., 2019. Diethanolamine functionalized rice husk for highly efficient recovery of gallium(III) from solution and a mechanism study. Mater. Sci. Eng. C 99, 1115–1122. https://doi.org/10.1016/j.msec.2019.02.028.

Zhang, L., Ruiz-Menjivar, J., Tong, Q., Zhang, J., Yue, M., 2021. Examining the carbon footprint of rice production and consumption in Hubei, China: A life cycle assessment and uncertainty analysis approach. J. Environ. Manage. 300,. https://doi.org/10.1016/j.jenvman.2021.113698 113698.

Zhao, D., Wang, Z., Lu, S., Shi, X., 2020. An amidoxime-functionalized polypropylene fiber: Competitive removal of Cu(II), Pb(II) and Zn(II) from wastewater and subsequent sequestration in cement mortar. J. Clean. Prod. 274,. https://doi.org/10.1016/j.jclepro.2020.123049 123049.

Zhu, Y., Hu, J., Wang, J., 2012. Competitive adsorption of Pb(II), Cu(II) and Zn(II) onto xanthate-modified magnetic chitosan. J. Hazard. Mater. 221–222, 155–161. https://doi.org/10.1016/j.jhazmat.2012.04.026.